Investigation of a Gallium MPD Thruster with an Ablating Cathode

Robert E. Thomas[1], Rodney L. Burton[2]
University of Illinois, Urbana, IL, 61801

Kurt A. Polzin[3]
NASA-Marshall Space Flight Center, Huntsville, AL 35812

The coaxial gallium electromagnetic (GEM) thruster [AIAA-2008-5021, IEPC-2009-233] uses a flat-top high-current pulse to enable operation at high exhaust velocities (~ 20 km/s). Gallium appears to offer several advantages over propellants currently in use. The non-toxicity and liquid temperature range (30 °C – 2204 °C) provide numerous feed system advantages, while the high atomic mass and low ionization potential (5.99 eV) predict low frozen flow losses. In addition, mass injection is controlled by the arc, eliminating the need for pulsed gas valves.

In the present experiment, a low energy spark igniter pre-ionizes propellant from a central 8.7 mm diameter gallium cathode, and the ablation products expand radially towards the inner walls of the outer stainless steel electrode. When the gallium bridges the electrodes, it effectively acts as a switch causing the main discharge to commence, with the Lorentz force accelerating the gallium plasma axially to produce thrust. The thruster is powered using fifty 88 μF, 1.2 kV capacitors in a 10-stage pulse forming network (PFN). A photograph of the thruster is shown in Fig. 1.

Radial and axial triple Langmuir probe measurements are made as a function of the discharge current. The triple probe consists of three 0.381 mm (0.015") diameter tungsten wires fed through a four-bore alumina tube with an O.D. of 4.7 mm. The electron density is found to be on the order of 10^{21}-10^{22} m^{-3} while the electron temperature varies from 3-5 eV. The radial and axial probe sweeps are used to calculate the divergence cone angle. The electron temperature and density data also permit the calculation of the electron-electron mean free path, which suggests that local thermodynamic equilibrium exists at the face of the cathode surface. The Saha equation is used assuming step-wise ionization to calculate the degree of ionization. It is found that at the face of thruster the gallium is fully doubly ionized. The electron temperature and density measurements as a function of current are used in the cathode spot (power balance) model described below.

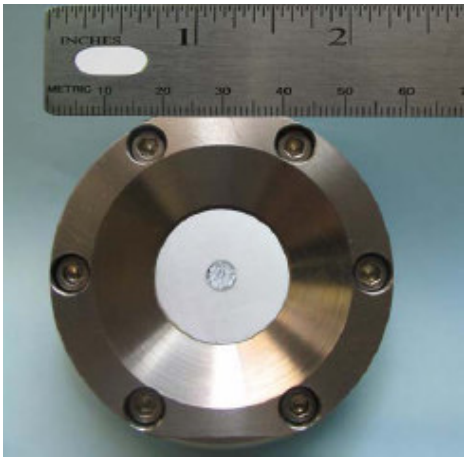

Figure. 1. Coaxial GEM Thruster.

[1] Graduate Research Assistant, Department of Aerospace Engineering. NASA-Graduate Student Research Program.
[2] Professor, Department of Aerospace Engineering.
[3] Propulsion Research Scientist, Propulsion Research and Technology Branch, Propulsion Systems Dept.

A power balance calculation is performed at the cathode surface in order to calculate the mass flow rate as a function of the discharge current. In the model it is assumed that the surface is heated by the bombardment of ions and back-diffusing electrons, and the power is dissipated through heat conduction, thermofield (electron) cooling, and evaporation. An expression for the electric field is derived through the integration of Poisson's equation. The ion current fraction $s = j_i/j_{tot}$ is also calculated from the model. The net heavy particle flux Γ (m^{-2}-s^{-1}) is taken to be the evaporated atomic flux minus the flux of ions deposited on the cathode surface

$$\Gamma_{net} = \Gamma_{vap} - \Gamma_{ion} \qquad (1)$$

The calculated mass flow rate is shown to be in good agreement with the experimental values (Fig. 2). The model below assumes a parabolic radial distribution of the current density. Other radial distributions are also explored. The calculated mass flow rate assumes that all of the gallium mass is ablated in the form of a vapor. A witness plate is placed in front of the thruster and microscopically examined in order to detect the presence of gallium macroparticles.

The power balance model is consistent with cathode spots that carry 100-200 A of current with high local temperatures (> 3000 K) and electric fields (> 10^8 V/m). These high temperatures and field values support substantial thermofield emission such that the electrons carry over half of the discharge current. It can also be seen from Fig. 2 that the mass flow rate varies quadratically with the discharge current. It has been shown [IEPC-2009-233] that the exhaust velocity is therefore independent of the current. The efficiency of the thruster can be expressed as the ratio of the dynamic impedance to the arc impedance: $\eta = Z_{dyn}/Z_{arc}$. These quantities can be expressed in terms of the inductance ratio, arc impedance and mass bit:

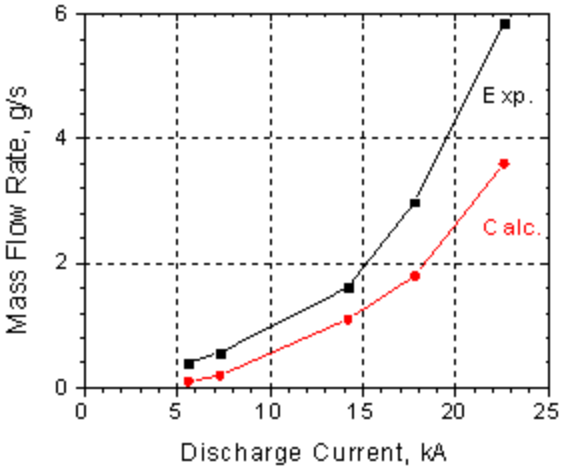

Fig. 2. Experimental and calculated mass flow rate as a function of current.

$$\eta = \frac{(L')^2 \psi}{8 m Z_{arc}} \qquad (2)$$

where L' is the inductance-per-unit-length, which is a function of the electrode radius ratio. From equation 2it can be seen that increasing the electrode radius ratio increases the efficiency of the thruster. Mass bit, discharge current and arc voltage measurements are obtained for thrusters possessing three different electrode radius ratios for comparative purposes. Increasing the radius ratio to 5 yields a thruster efficiency of 40% with an exhaust velocity of 23 km/s.

A B-field probe diagnostic is employed in the discharge region. The probes are constructed of 4 turns of 36 AWG wire with a core diameter of 0.9 mm. The probe signals are numerically integrated to yield B(t). Once the spatial distribution of the magnetic field is known, the current density distribution can be mapped, and the ion Larmor radius can be calculated. The Larmor radius is an important parameter in the performance of MPD thrusters. It has been shown [AIAA-2007-5855] that for efficient operation of MPD thrusters the Larmor radius must be smaller than radius of the outer electrode. The magnetic field measurements in addition to the calculation of the ion charge state Z, and ion current fraction j_i show that ion Larmor radius is small enough when the discharge current level is 23 kA.

Investigation of a Gallium MPD Thruster with an Ablating Cathode

Robert E. Thomas* and Rodney L. Burton †

University of Illinois, Urbana, IL, 61801

Kurt A. Polzin‡

NASA-Marshall Space Flight Center, Huntsville, AL, 35812

Arc impedance, exhaust velocity, and plasma probe measurements are presented. The thruster is driven by a 50 μs pulse from a 6.2 mΩ pulse forming network, and gallium is supplied to the discharge by evaporation of the cathode. The arc voltage is found to vary linearly with the discharge current with an arc impedance of 6.5 mΩ. Electrostatic probes yield an exhaust velocity that is invariant with the discharge current and has a peak value of 20 km/s, which is in reasonable agreement with the value (16 $\pm$ 1 km/s) calculated from the mass bit and discharge current data. Triple probe measurements yield on axis electron temperatures in the range of 0.8-3.8 eV, electron densities in the range of 1.6 $\times$ 10^{21} to 2.1 $\times$ 10^{22} m^{-3}, and a divergence half angle of 16°. Measurements within the interelectrode region yield a peak magnetic field of 0.8 T, and the observed radial trends are consistent with an azimuthally symmetric current distribution. A cathode power balance model is coupled with an ablative heat conduction model predicting mass bit values that are within 20% of the experimental values.

Nomenclature

A	= Area, m^2	r	=Radius, m
B	= Magnetic Field, T	s	= Electron current fraction
c	= Constant; ion speed, m/s	S	= Ablated surface position, m
D	= Electron tunneling function	t	= Time, s
e	= Elementary charge, C	T	= Thrust, N; Temperature, K
H	= Enthalpy, J	u_e	= Exhaust velocity
I	= Discharge Current, A	V	= Voltage, V
j	= Current density, A-m^{-2}	Z	= Ion charge number
k	= Boltzmann's Constant, J/K	β	= Empirical ablation exponent
L	= Inductance, H	χ	= Non-dimensional potential
m	= Mass, kg	ϕ	= Potential, V
M	= Molar Mass, kg/mol	μ_o	= Vacuum permeability, H/m
n_e	= Electron density, m^{-3}	ρ	= Density kg-m^{-3}
N	= Electron supply function	Γ	= Gamma function; atomic mass flux, m^{-2}–s^{-1}
p	= Pressure, Pa	Ψ	= Current action integral, A^2-s
P	= Power, W		

*Graduate Research Assistant, Department of Aerospace Engineering, Member AIAA.

†Professor, Department of Aerospace Engineering, Associate Fellow AIAA.

‡Propulsion Research Scientist, Propulsion Research and Technology Applications Branch, Propulsion Systems Dept., Senior Member AIAA

I. Introduction

The gallium electromagnetic (GEM) thruster uses a high-current arc discharge to ablate and accelerate liquid metal propellant to high exhaust velocities (15-20 km/s). Previous studies have detailed the GEM concept and design,[1] with data for both a low energy[2] (20 J/ per pulse) and MW- level quasi-steady gallium thruster.[3,4] In the present study, arc impedance and mass measurements are presented for discharge currents in the range of 6 - 23 kA. A series of electrostatic probes are used to measure the axial variation of the exhaust velocity. Triple probe data are used to map the exhaust plume and calculate the plume divergence half-angle, and magnetic field probing near the cathode tip is used to infer the radial distribution of the axial current into the electrode. A cathode power balance and 1-D heat conduction model are used to calculate the mass flow rate.

II. Experimental Apparatus

II.A. Testing Facilities

Tests were conducted at the University of Illinois Electric Propulsion Laboratory on the coaxial GEM thruster shown in Fig. 1. The stainless steel annular electrode has an inner diameter of 30 mm, and the 8.7 mm diameter gallium electrode is insulated by boron nitride. The thruster is mounted into a 5-way vacuum cross, which is attached to the main vacuum chamber. A baffle is inserted into the 5-way cross to condense and capture ejected gallium particles before they reach the main chamber. Vacuum was maintained by a TPH1500 turbomolecular pump, which was backed by two Roots blowers and two Kinney mechanical displacement pumps. The base pressure of the facility during testing was 5×10^{-5} torr.

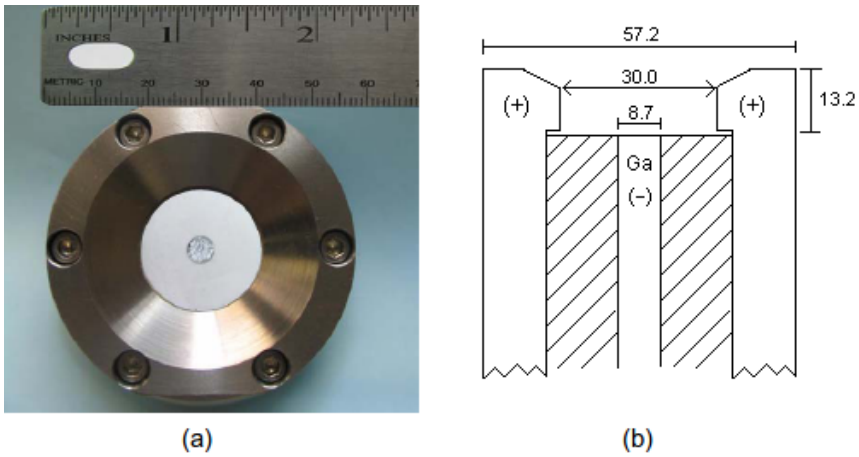

Figure 1. (a) Photograph and (b) schematic of coaxial GEM thruster (dimensions in mm).

A ten-section, 5-line pulse forming network (PFN) was used to power the thruster. Each of the 5 sections consists of ten 88 μF capacitors in series with 85 nH inductors. The 50 capacitors have a maximum charging voltage of 1.2 kV, which yields a bank energy of 3.2 kJ, capable of creating a 100 kA $\times$ 50 μs current pulse. The maximum current used for the present experiments was 23 kA for a bank energy of 270 J. A copper sheet with punched holes was located over the capacitors to provide a common ground (ground plane). Brass standoffs with a height of 3.8 cm were machined to provide spacing between the stage inductors and the ground plane. Two 9 cm long, 0.32 cm (1/8") diameter copper rods yield a section inductance of 85 nH. The five PFN lines were each connected in parallel using 2.5 cm wide copper strip. To minimize stray inductance in the charging circuit, the PFN was mounted close to the vacuum chamber, as shown in Fig. 2. A 7.0 cm wide strip of copper sheet formed the transmission line to the thruster. The capacitors were charged using a Hipotronics DC power supply.

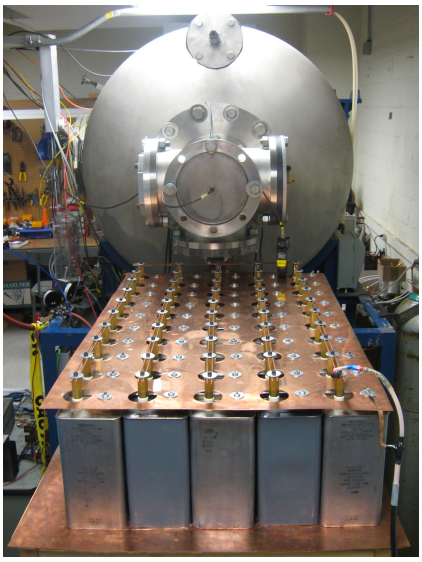

Figure 2. 3.2 kJ Pulse Forming Network and 1.5 m^3 vacuum tank.

III. Experimental Results

III.A. Voltage and Current Measurement

Measurements were obtained for capacitor charging voltages in the range of 150-350 V. A Pearson 4418 current monitor and Tektronix P6015A voltage probe were used to measure the discharge current and terminal voltage. Typical discharge current and arc voltage waveforms are shown in Fig. 3, for $E_o = 270$ J. The PFN impedance is well-matched to the arc impedance, with greater than 90% of the capacitor energy being transferred to the discharge.

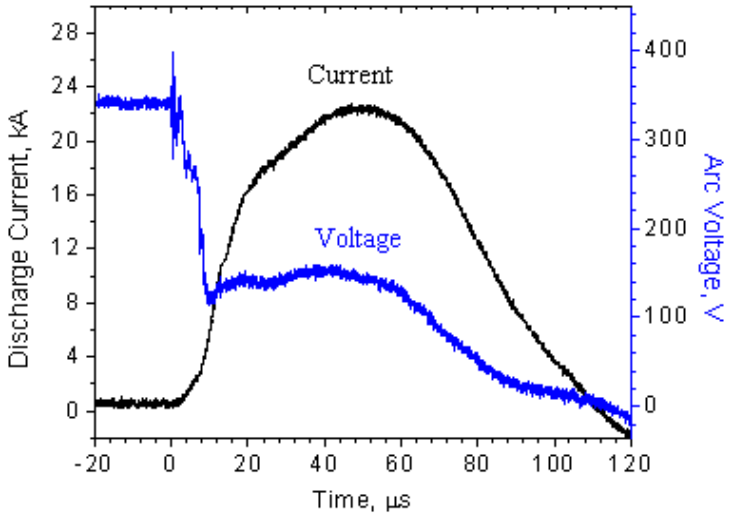

Figure 3. Discharge current and arc voltage trace taken at $E_o = 270$ J.

The voltage is plotted as a function of the discharge current in Fig. 4 for two different electrode radius ratios. In both cases the voltage varies linearly with the discharge current with arc impedance values in the range of 6.5 - 7.2 mΩ. No evidence of the high-current onset phenomena is seen at any current level.

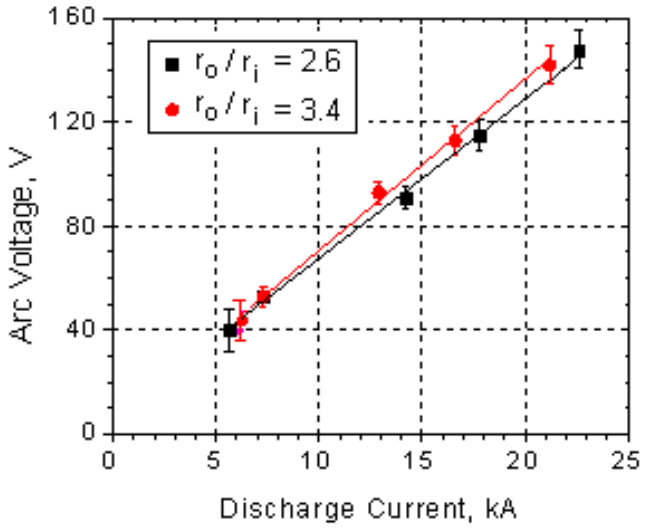

Figure 4. Arc Voltage plotted against the discharge current for two different electrode radius ratios.

III.B. Mass Bit Measurement

The mass ablated per pulse was measured by weighing the central and annular electrodes after a prescribed number of shots using a Mettler AG245 measurement scale with a resolution of 0.1 mg. Several hundred shots were fired which liberated at least 10 mg, leaving the error due to instrumentation at less than 1%. Tests were repeated 10 times at each energy level, and the ablated mass measurements were found to be highly repeatable. No visible oxidation was seen on the solid gallium surface before or after testing. The mass of the annular stainless steel electrode decreased slightly after each test run. However, the total amount of mass lost (i.e. 0.3 mg after 250 shots) was less than 1% of the total ablated mass. Gallium macroparticle ejection prevented use of a central gallium anode[4] and limited the discharge current to 22.6 kA (equivalent to a uniform current density of $j = 3.7 \times 10^8$ A/m^2) when using a central cathode. A photograph of the macroparticles is shown in Fig. 5.

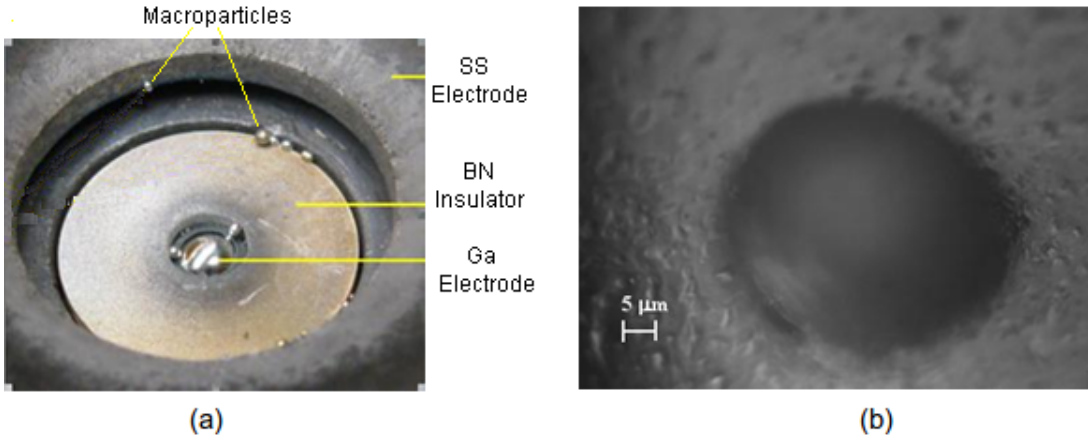

Figure 5. (a) Gallium macroparticles deposited on insulator and outer electrode after firings with a central anode, (b) corresponding SEM photograph of post-mortem crater left on gallium surface.

The mass ablated per pulse is shown in Fig. 6 as a function of the current action integral Ψ, defined as

$$\Psi = \int_0^{t_p} I^2(t)\, \mathrm{d}t \tag{1}$$

The slope in Fig. 6 is proportional to exhaust velocity, which has a value of 16 $\pm$ 1 km/s.

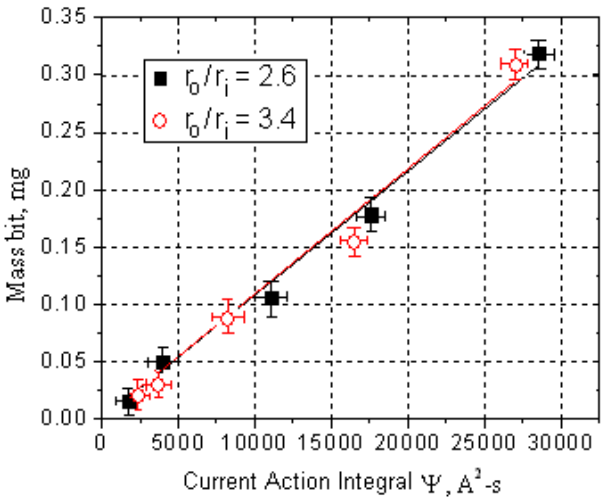

Figure 6. Measured mass bit vs. current action integral for electrode radii ratios of 2.6 and 3.4.

The ($m \propto I^2$) mass measurement is consistent with the linearity of the V-I characteristic. This can be seen through examination of the electromagnetic scaling relations, assuming the mass flow rate follows a power law dependence on the discharge current

$$\dot{m} \propto I^{\beta} \tag{2}$$

where β is an empirical parameter (equal to zero for gas-fed thrusters). Recalling the electromagnetic thrust relation[5]

$$T = \frac{1}{2} L' I^2, \text{where } L' = \frac{\mu_o}{2\pi}\left(\ln\frac{r_o}{r_i} + \frac{1}{2}\right) \tag{3}$$

The following relations are easily found

$$P = IV_{arc} \propto \frac{1}{2}\dot{m}u_e^2;\ V_{arc} = I^{3-\beta};\ \text{and } u_e \propto I^{2-\beta} \tag{4}$$

Equation (4) has been applied[4] to three ablative thrusters: a graphite MPD,[6] Teflon MPD,[7] and a Teflon PPT.[8] The mass bit was found to vary quadratically with the discharge current for both MPD thrusters, and the measured velocity was invariant with the discharge current. Similar trends were found for the GEM thruster, as described in the following section.

IV. Exhaust Velocity Measurements

The exhaust velocity of the gallium plasma was measured using both a time of flight (TOF) technique, and a crossed electrostatic probe measurement. The TOF technique was employed by using a pair of floating double probes placed perpendicular to the flow. By measuring the time between local ion fluctuations, a velocity can be inferred. A sample double probe trace is shown in Fig. 7.

The crossed electrostatic probe utilizes cylindrical probes placed parallel and perpendicular to the velocity flow vector. In a flowing plasma, the ion current collected by the probe is a function of the angle between the longitudinal probe axis and the plasma velocity vector. Assuming a Maxwellian velocity distribution and a thin cylindrical sheath, the current collected in a flowing plasma by a cylindrical probe is given by[9]

$$I = \left(\frac{kT}{2\pi m}\right) n_e e A \frac{2}{\sqrt{\pi}} \exp(-(\kappa)^2) \sum_{n=0}^{\infty} \left(\frac{\kappa^n}{n!}\right)^2 \Gamma\left(n + \frac{3}{2}\right) \tag{5}$$

where $\kappa = v/c_m \sin(\theta)$ and Γ is the gamma function. The ratio v/c_m is the ratio of the local flow velocity to the most probable ion thermal speed and θ is the angle between the probe axis and the velocity flow vector. By comparing the signals obtained from a probe placed both parallel and perpendicular to the plasma flow,

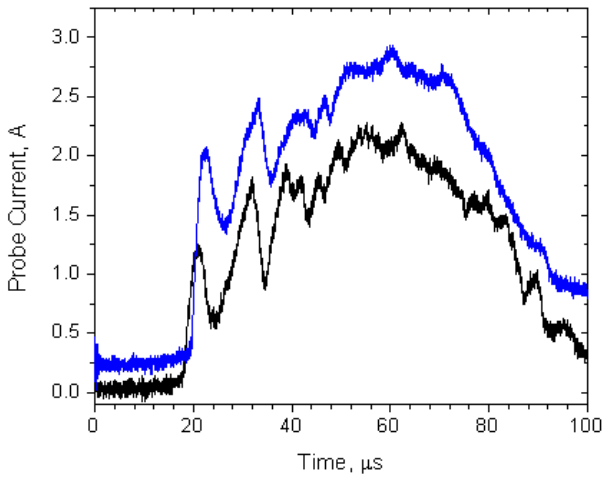

Figure 7. TOF double probe trace obtained at an axial distance of 12 cm from the thruster exit plane.

the ratio v/c_m can be determined. It is determined experimentally that $I_\perp/I_{||} > 1$, so the velocity can be determined directly from the perpendicular probe current $I_\perp = Zen_e uA_p/\pi$ to within 3% accuracy.[9] Figure 8 shows the axial variation of the exhaust velocity and the velocity as a function of the discharge current. The velocity calculated from the mass bit and discharge current (16 km/s) is within the error bars of both probes, and the velocity is found to be invariant with the discharge current, which is consistent with $\beta = 2$ from the mass measurements.

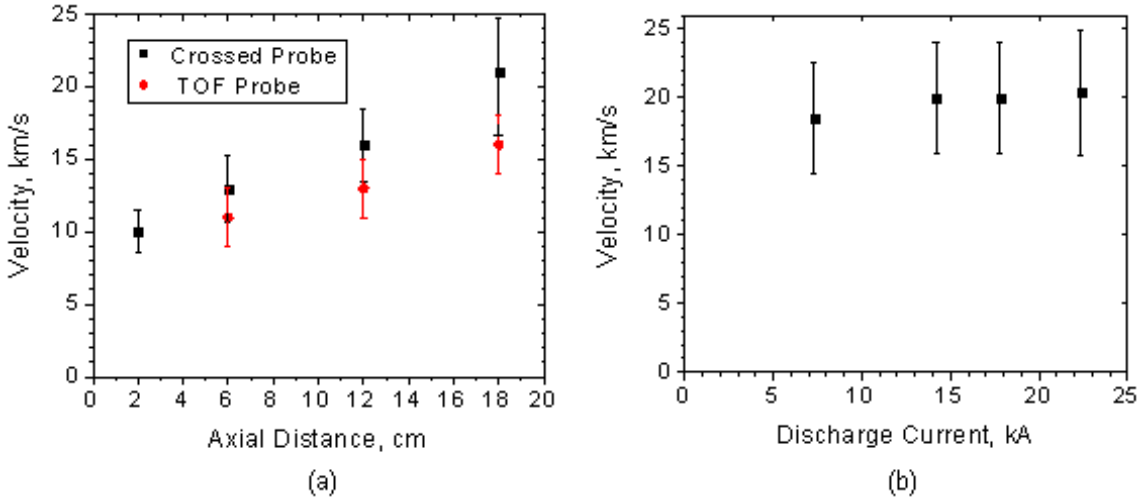

Figure 8. (a) Axial variation of crossed probe and TOF velocity, (b) Crossed probe velocity as a function of discharge current.

V. Triple Probe Measurements

The triple Langmuir probe, and its variant the quadruple probe, have been used extensively in MPD and PPT plumes to determine the electron density and temperature.[10–13] The triple probe used in this study consists of three 0.19 mm tungsten wires with an exposed length of 5.0 mm and a probe separation distance of 1.0 mm. Two floating voltages ϕ_{d2} and ϕ_{d3} are supplied by using lead-acid rechargeable batteries. The probe currents were measured using 1:1 Pearson current transformers. A photograph and schematic of the triple probe are shown in Fig. 9.

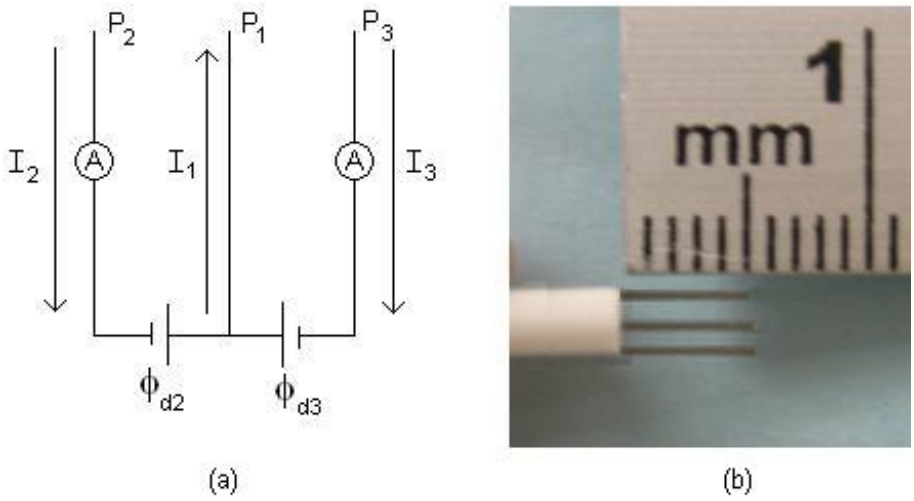

Figure 9. (a) Schematic of triple probe circuit and (b) photograph of probe.

The theory of triple probes is detailed in Ref. [14]. The currents collected by each probe are given by

$$\begin{aligned} -I_1 &= -A_p j_e \exp(\chi_1) + A_p j_i(\chi_1) \\ I_2 &= -A_p j_e \exp(\chi_2) + A_p j_i(\chi_1) \\ I_3 &= -A_p j_e \exp(\chi_3) + A_p j_i(\chi_1) \end{aligned} \tag{6}$$

where A_p is the probe area. The electron j_e and ion j_i current densities are given by

$$j_e = n_e e \left(\frac{kT_e}{2\pi m_e} \right)^{1/2} \tag{7}$$

$$j_i = \exp\left(-\frac{1}{2}\right) e n_e \left(\frac{kT_e}{m_i} \right)^{1/2} \tag{8}$$

and the non-dimensional potential χ is given in terms of the space potential ϕ_p by

$$\chi \equiv \frac{e(\phi - \phi_p)}{kT_e} \tag{9}$$

Equations (6) - (9) are used to find the electron temperature, density, and plasma potential. Collected probe currents are shown in Fig. 10, and the axial variation in the electron density and temperature are shown in Fig. 11. The electron temperature has a peak value of 3.6 eV, and this value is used in the power balance model described below. The electron density has a peak value of 2.1×10^{22} m^{-3}, and drops by roughly a factor of 10 at a distance of 18 cm. A divergence plume half-angle of 16° is calculated through use of the continuity equation $n_e A u_e = \text{const}$, using measured values of the axial electron density and velocity. The radial variation of the electron density and temperature is shown in Fig. 12. The density exhibits very little radial divergence between the two axial stations, while the temperature drops by a factor of two as the probe is moved radially from the centerline of the thruster. The drop in electron temperature at the plasma edge is likely due to diffusion and radiative cooling at the plasma edge.

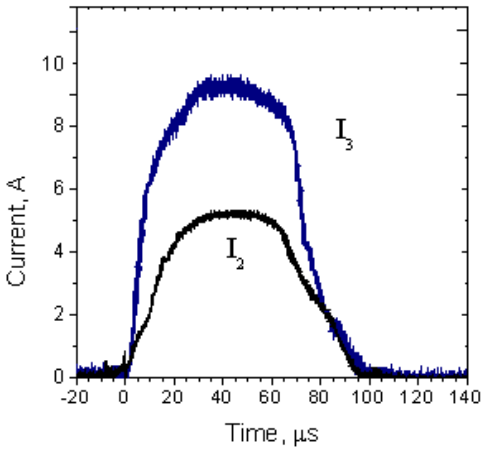

Figure 10. Collected triple probe currents taken 2 cm from exit plane of the thruster.

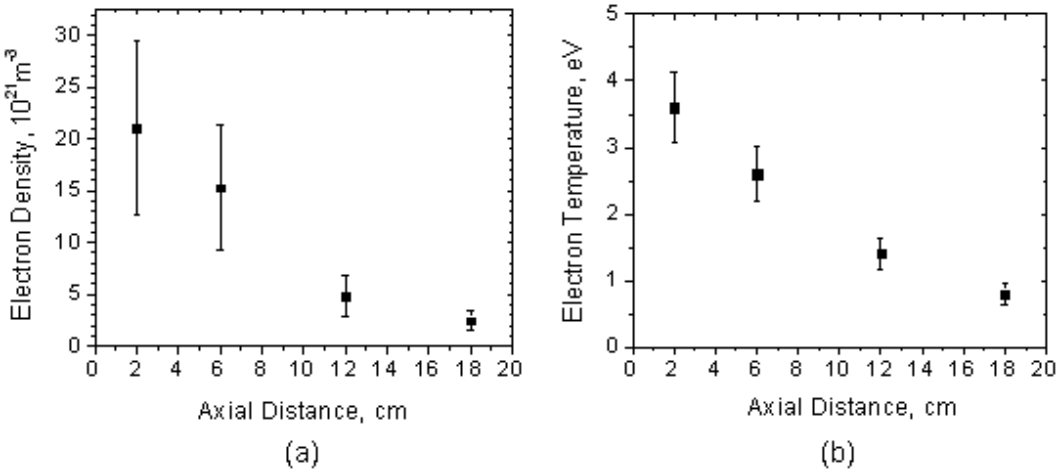

Figure 11. Axial variation of the (a) electron density and (b) electron temperature for $E_o = 270J$.

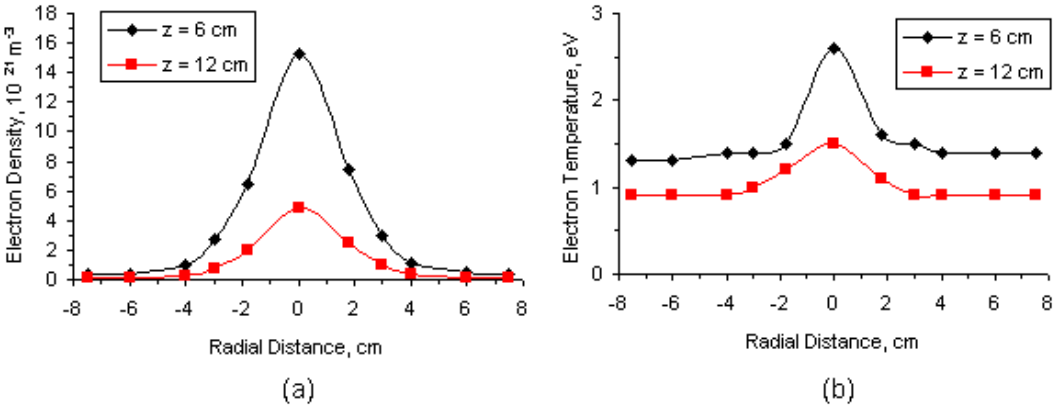

Figure 12. Radial variation of the (a) electron density and (b) electron temperature taken at an axial distance of 6 and 12 cm from the exit plane of the thruster

VI. Magnetic Field Probe Measurements

A radial trace of the magnetic field was made along the face of the cathode using a 3-turn magnetic field coil. The coil has a diameter of 0.9 mm and is enclosed within a 1.4 mm Pyrex tube. A photograph of the

probe and a numerically integrated signal are shown in Fig. 13.

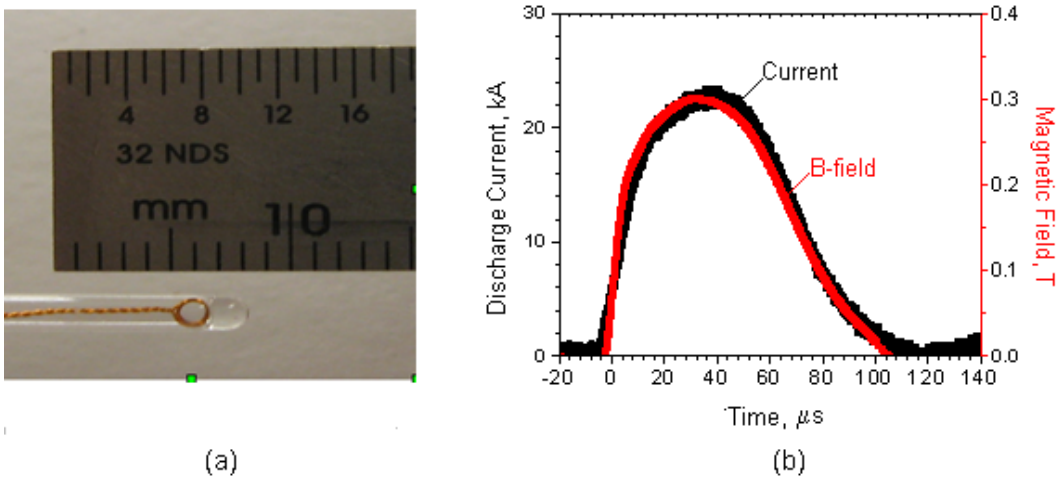

Figure 13. (a) Photograph of 3-turn b-dot probe and (b) integrated b-dot signal taken at r = 1.5 cm at a discharge current of 22.6 kA.

Magnetic field probe data are obtained at 7 radial locations along the insulator and cathode surface and are presented in Fig. 15. The trends in the observed data can be compared with the relations derived assuming a uniform axial current, as shown in Fig. 14.

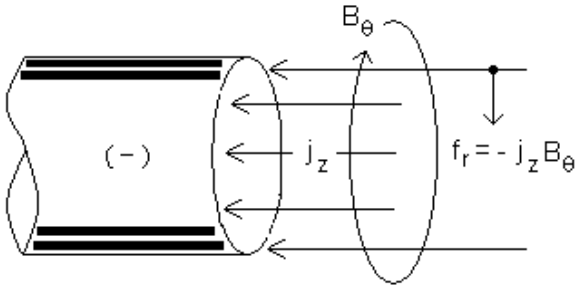

Figure 14. Current density model assuming a uniform, axial current.[5]

The pressure profile across the cathode surface is given by

$$p(r) = \frac{\mu_o I^2}{8\pi^2 r_c^2}\left[1 - \left(\frac{r}{r_c}\right)^2\right] \tag{10}$$

Ampere's law can be manipulated for a uniform radial current at the cathode face to show

$$B_\theta = \begin{cases} \frac{\mu_o I}{2\pi r_c^2} r & \text{for } r \le r_c, \\ \frac{\mu_o I}{2\pi r} & \text{for } r \ge r_c. \end{cases} \tag{11}$$

The two linear regions found in Fig. 14 are consistent with equation 11, with excellent quantitative agreement near the inner edge of the anode (r = 15 mm). The measured magnetic field along the centerline is non-zero; this can be attributed to the finite size of the probe and the corresponding plasma perturbation.

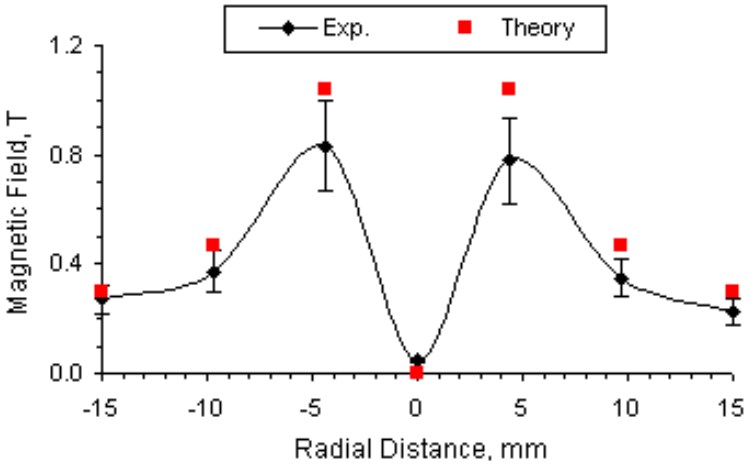

Figure 15. Radial trace of the experimental and theoretical magnetic field data. The dotted line denotes the outer boundaries of the gallium cathode.

The magnetic field can be used to calculate the ion Larmor radius, defined as

$$r_L = \frac{m_i u}{ZeB} \tag{12}$$

The radial variation in the Larmor radius is shown in Fig. 16, based on a $Z = 3$ plasma, which is calculated from the triple probe data. We estimate the Larmor radius during the acceleration process, so that $u < u_e$. For example, for $u_e = 16$ km/s, we calculate r_L at 50% of u_e, or 8 km/s, The Larmor radius within the interelectrode region is less than the radius of the outer electrode (15 mm), which is advantageous from the standpoint of efficiency .

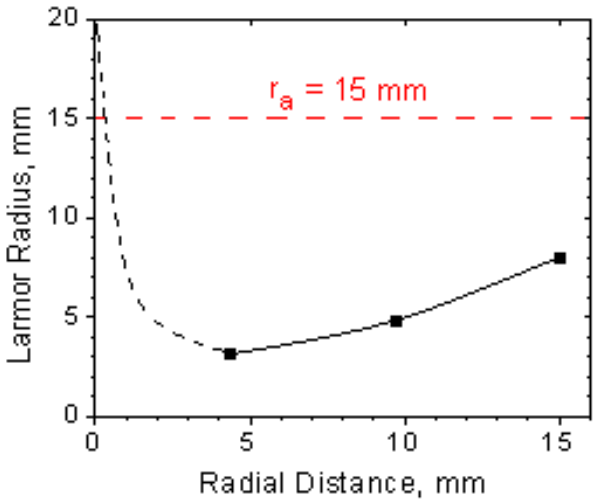

Figure 16. Radial variation of the Larmor radius, calculated from measured magnetic field probe data.

This Larmor radius result has important implications for the ion acceleration process, since ions at a radius larger than a few mm are effectively collisionless, and will execute $\mathbf{E} \times \mathbf{B}$ drift. Because of the large radial $\mathbf{E}$ field created by the electrode geometry (Fig. 1) the drift is predominantly axial with a small radial component, and accounts for the measured exhaust velocity and small divergence of the exhaust beam

VII. Cathode Power Balance and Heat Conduction Model

In this section a cathode power balance and ablative heat conduction model are used to estimate the mass flow rate as a function of discharge current. Similar calculations have been used to successfully model

vacuum arcs,[15] high-pressure arc systems using non-refractory electrodes,[16] arcjet thrusters,[17] and MPD thrusters employing a refractory cathode. The discharge current is assumed to enter the cylindrical cathode as a uniform axial beam (Fig. 14). The atomic flux of evaporated gallium atoms is given by

$$\Gamma = \frac{P_v}{\sqrt{2\pi m_i k T_s}} \tag{13}$$

where P_v is the vapor pressure and T_s is the surface temperature. The surface temperature is found from the ablative heat conduction model described below, and the vapor pressure is set equal to the pinch pressure (equation 10). Several studies have been conducted on the relationship between the metallic vapor pressure and magnetic pinch pressure in high-current arcs. Maecker[18] found reasonable agreement between the calculated magnetic pressure and the measured forces on the carbon electrodes of an electric arc. Lee[19] and Schrade et al.[20] have provided stability criteria which suggests that the vapor pressure has to exceed the magnetic pinch pressure in the vicinity of the cathode surface. Setting the pinch pressure equal to the vapor pressure, the mass flow rate is given by

$$\dot{m}_{net} = \dot{m}_{out} - \dot{m}_{in} = c\sqrt{\frac{M}{T_s}} I^2 - \frac{(1-s) I m_i}{Ze} \tag{14}$$

where the constant c has a value of 0.66×10^{-9} for a flat surface and s is the electron current fraction. The expression for the outflux of gallium atoms uses a modified form[20] of equation (13) , while the second term represents the flux of ions that return to the gallium surface. The physical model developed by Coulombe and Meunier[16] for non-refractory, vaporizing electrodes serves as the basis for the current study. The gallium cathode is heated through bombardment of ions, and to a lessor extent, highly energetic plasma electrons. The cathode is cooled through heat conduction, evaporation, and the emission of thermofield electrons. Current continuity is given by

$$j_{tot} = j_{ion} + j_{bde} + j_{tf} \tag{15}$$

where j_{ion}, j_{bde}, and j_{tf} are the ion, back diffusing electron, and thermofield current densities, respectively. The ion current density is found through use of Bohm's criteria for sheath formation,[21] assuming the ions enter the sheath at the local sound velocity c_s

$$j_{ion} = \sum_i Z e n_i c_s \tag{16}$$

The back-diffusing plasma electron current density is given by

$$j_{bde} = \frac{1}{4} e n_e \exp\left(-\frac{e\phi_c}{kT_e}\right) v_e \tag{17}$$

where v_e is mean electron velocity, and ϕ_c is the cathode sheath potential. The thermofield electron emission is due to the high temperature and electric field present at the cathode surface

$$j_{tf} = e \int_{-\infty}^{\infty} N(T_s, \epsilon) D(E, \epsilon)\ \mathrm{d}\epsilon \tag{18}$$

where expressions for the electron supply function $N(T_s, \epsilon)$ and electron tunneling probability $D(E, \epsilon)$ are given in Ref. [22]. In the limit of small electric fields, (18) reduces to the Richardson-Dushman equation, and in the limit of low temperatures, the Fowler-Nordheim equation. A power density balance across the cathode surface is given by

$$P_{ion} + P_{bde} + P_{joule} = P_{tf} + P_{vap} + P_{cond} + P_{rad} \tag{19}$$

where the terms on the left hand side represent heating terms, and the terms on the right hand side are cooling mechanisms (thermofield emission, evaporation, heat conduction, and radiative cooling). The heating terms (ion, electron, and Joule heating) can be expressed as

$$\sum_i j_i \left(\phi_c + \phi_i - Z\phi_{eff} + \frac{5kT_i}{2Ze}\right) + j_{bde}\left(\phi_{eff} + \frac{5kT_e}{2e}\right) + g\frac{I^2}{\sigma} r_c \tag{20}$$

where ϕ_i is the ionization potential, g is a geometric constant between 0.5-0.8, σ is the electrical conductivity, and ϕ_{eff} is the effective work function, which is found by subtracting the Schottky emission potential from the work function $\phi_{eff} = \phi_w - (eE/4\pi\epsilon_o)^{1/2}$. The ion current densities are found through use of the Saha equation using the experimentally found value of $T_e = 3.6$ eV. The cooling due to electron emission is given by[23]

$$P_{tf} = j_{tf}\left(\phi_{eff} + \frac{2kT_s}{e}\right) \tag{21}$$

Radiative cooling is given by (setting the emissivity = 1)

$$P_{rad} = \sigma T_s^4 \tag{22}$$

where σ is the Stefan-Boltzmann constant. The cooling due to evaporation is given by

$$P_{vap} = \pi^{-1} r_c^{-2}(H_{vap} + H_f)\dot{m} \tag{23}$$

where H_{vap} is the enthalpy of vaporization (2.6 eV/atom) and H_f the enthalpy of fusion (0.06 eV/atom).

The time dependent surface temperature and cooling due to heat conduction are found through an ablative heat conduction model. To simplify the analysis in such problems it is assumed that the ablated material is completely removed from the surface as soon as it evaporates. The analysis can be divided into two distinct regimes, depending on the the time needed to vaporize the gallium electrode t_{vap}. For $t < t_{vap}$, the problem is a standard heat conduction problem using boundary conditions for a semi-infinite solid. For $t > t_{vap}$, the electrode boundary surface $S(t)$ moves as ablation takes place due to charged particle bombardment P. Note that for a 23 kA pulse the ablated mass per pulse is 300 μg and $\Delta S = 0.8$ microns. The location of the solid boundary surface during ablation is shown in Fig. 17.

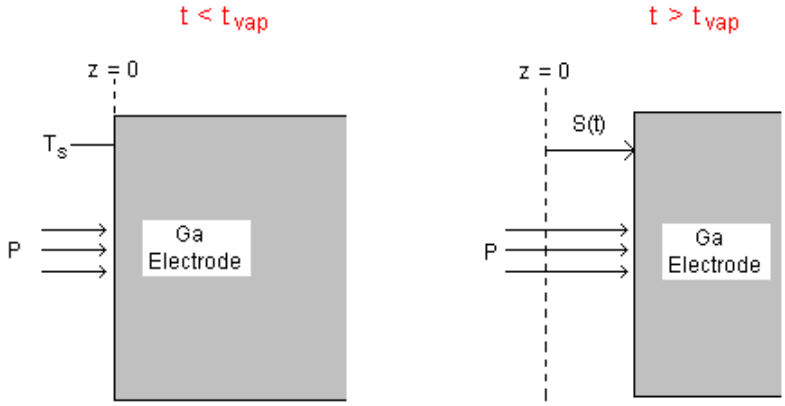

Figure 17. 1-D ablation model used to calculate the surface temperature.

The heat conduction in terms of the enthalpy is given by[24]

$$\frac{\mathrm{d}}{\mathrm{d}t}\int \rho H \, \mathrm{d}z = \left(k\frac{\partial T}{\partial z} - P\right) \tag{24}$$

where ρ and λ are the density and thermal conductivity. The boundary condition at the ablating surface is found by equating the net heat flux entering the boundary surface to the energy absorbed as a result of ablation per unit time per unit area

$$-k_+\frac{\partial T_+}{\partial z} = P - \rho H_{vap}\frac{\mathrm{d}S}{\mathrm{d}t} \tag{25}$$

where the + denotes that the values are the limits within the cathode surface. The energy equation is first solved in its enthalpy form and the temperature is back-calculated afterwards. The system of equations is closed by using an expression for the electric field, which is found through integration of Poisson's equation[25]

$$\varepsilon_o \frac{E^2}{2} = -|j_{tf}|\sqrt{\frac{2m_e\phi_c}{e}} - \frac{|j_i|}{e}\sqrt{m_i kT_e}\left(1-\left(\frac{2Ze\phi_c}{kT_e}+1\right)^{1/2}\right) - Z\frac{|j_{ion}|}{e}\sqrt{m_i kT_e}\left(1-\exp\left(-\frac{e\phi_c}{kT_e}\right)\right) \quad (26)$$

The temperature, electric field and ion current fraction are shown in Fig. 18. As expected, the ions carry the bulk of the current at the cathode surface, and the surface temperature and electric field are insufficient for significant thermofield emission. The model yields cathode sheath potentials in the range of 13 - 17 V, which is roughly 2-3 times the ionization potential.

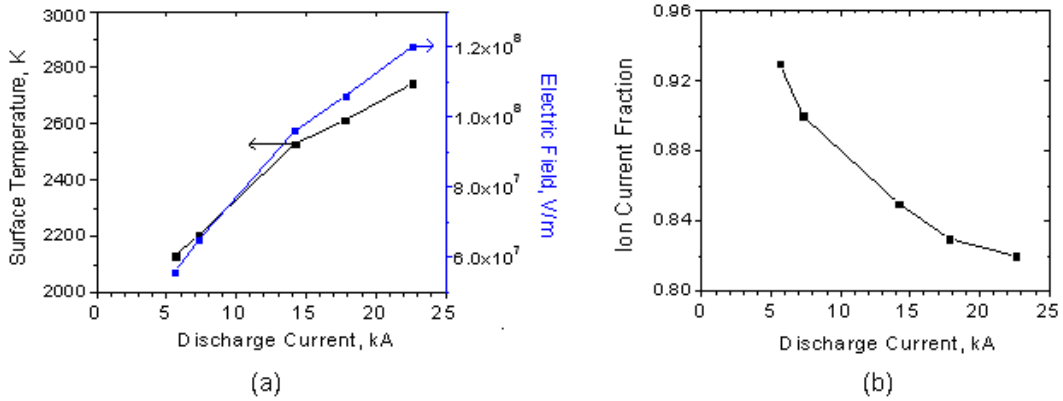

Figure 18. (a) Surface temperature and electric field and (b) ion current fraction as a function of discharge current.

The ablated mass is shown in Fig. 19. The calculated mass is roughly 20% less than the measured value. providing favorable quantitative agreement.

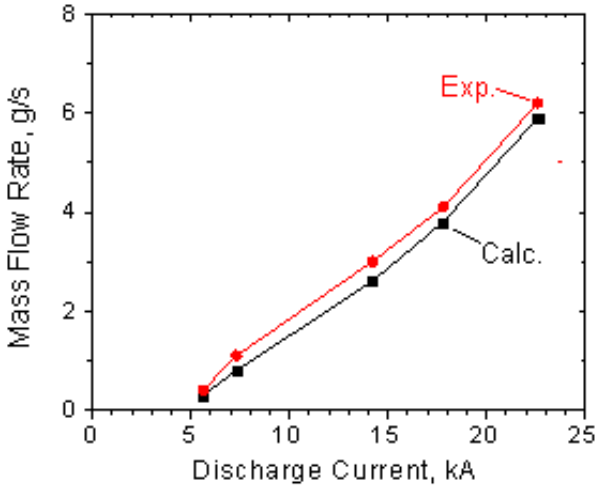

Figure 19. Comparison of the experimental and calculated mass flow rates as a function of discharge current.

VIII. Thruster Efficiency

The thruster efficiency of electric propulsion thrusters is given by the ratio of the jet kinetic power to the input power

$$\eta_t = \frac{\dot{m}u_e^2}{2P} \quad (27)$$

An equivalent form of the efficiency can be found by taking the dot product of Ohm's Law, which shows the total power is the sum of the dynamic and resistive components

$$\mathbf{j} \cdot \mathbf{E} = \eta j^2 + \mathbf{u} \cdot \mathbf{j} \times \mathbf{B} \tag{28}$$

The resistive component is found by dividing the arc voltage by the discharge current. The dynamic impedance is found through the relation $IZ_{dyn}^2 = (1/2)Tu_e$. The exhaust velocity is calculated from the mass bit and discharge current data

$$u_e = \frac{\int T dt}{m} = \frac{1}{2}\frac{L'\Psi}{m} \tag{29}$$

The efficiency can thus be expressed as the ratio of the dynamic to resistive impedance

$$\eta = \frac{Z_{dyn}}{Z_{arc}} = \frac{(1/4)L'u_e}{Z_{arc}} = \frac{(L')^2\Psi}{8mZ_{arc}} \tag{30}$$

The efficiency as a function of the electrode radius ratio is shown in Fig. 20. The radius ratios of 2.6 and 3.4 correspond to experimental values. As the radius ratio exceeds 5, the MPD thruster becomes prone to the spoking instability.

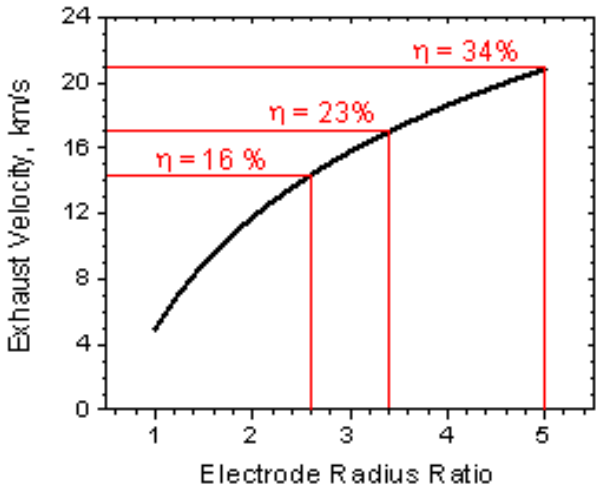

Figure 20. Exhaust velocity and thruster efficiency as a function of electrode radius ratio.

VIII.A. Discussion

A previous review of MPD performance [2] presented two parameters of interest: the ion Larmor radius R_L, and the charge carrier parameter α, which represents the fraction of the discharge current that can be carried by the number of ions present

$$\alpha = \frac{Ze}{mI}\frac{dm}{dt} \tag{31}$$

It is desirable to operate at a discharge current high enough to keep the Larmor radius smaller than the outer electrode radius, and for the present experiments with gallium, the Larmor radius criterion is easily satisfied (Fig. 16), and $\alpha = 1.1$ for $I = 23$ kA. The efficiency suffers however, from the high frozen flow loss of the triply ionized gallium.

IX. Conclusions

The results obtained can be summarized as follows:

- MPD thrusters require short pulses in order to reduce PFN mass, while gas-fed MPDs cannot reliably achieve switching for valved pulses less than 1000 μs. The present experiment successfully injects propellant through cathode ablation for a PFN pulse length of 50 μs.
- Experiments were conducted at discharge currents in the range of 6-23 kA utilizing a central gallium cathode. The arc voltage varies linearly with the discharge current with arc impedance values of 6.5 mΩ.
- The measured mass bit follows a quadratic dependence ($m \propto I^2$) on the discharge current. Time-of-flight and a crossed electrostatic probe yield velocities of 15 and 20 km/s, respectively. These are in reasonable agreement with $u_e = 16 \pm 1$ km/s, calculated from the mass bit and discharge current data.
- Triple Langmuir probe measurements along the center-line of the thruster yield a peak electron temperature and density of 3.6 eV and 2.1×10^{22} m^{-3} two centimeters from the exit plane of the thruster. The axial measurements suggest a well collimated exhaust plume with a divergence half-angle of 16°, with a triply ionized plasma at the cathode surface.
- Magnetic field measurements are consistent with azimuthally symmetric current distribution (no spoking instability).
- A combined cathode power balance and ablative heat conduction model yield a calculated mass flow rate within 20% of the experimentally measured value.
- An efficiency of 23% is calculated from the mass bit and discharge current data. It is suspected that ionization is the dominant loss mechanism.

References

[1]Polzin, K., Markusic, T., Burton, R., Thomas, R., and Carroll, D., "Gallium Electromagnetic (GEM) Thruster Concept and Design," *AIAA-2006-4652*, 2006.

[2]Thomas, R., Burton, R., Glumac, N., and Polzin, K., "Preliminary Spectroscopic Measurements for a Gallium Electromagnetic (GEM) Thruster," *AIAA-2007-5855*, 2007.

[3]Thomas, R., Burton, R., and Polzin, K., "Preliminary Development and Testing of a Self-Injecting Gallium MPD Thruster," *AIAA-2008-5081*, 2008.

[4]Thomas, R., Burton, R., and Polzin, K., "Gallium Electromagnetic (GEM) Thruster Performance Measurements," *IEPC-2009-233*, 2009.

[5]Jahn, R. G., *Physics of Electric Propulsion*, McGraw-Hill Book Company, 1968.

[6]Ducati, A. and Jahn, R., "Investigation of Pulsed Quasi-Steady MPD Arc Jets," Tech. rep., NASA Langley Research Center, 1971.

[7]Paccani, G., Chiarotti, U., and Deininger, W., "Quasisteady Ablative Magnetoplasmadynamic Thruster Performance with Different Propellants," *Journal of Propulsion and Power*, Vol. 14, No. 2, 1998, pp. 254–60.

[8]Laystrom, J. and Burton, R., "Geometric Optimization of a Coaxial Pulsed Plasma Thruster," *AIAA-2003–5025*, 2003.

[9]Kanal, M., "Theory of Current Collection of Moving Cylindrical Probes," *J. Appl. Phys.*, Vol. 35, 1964, pp. 1697.

[10]DelMedico, S. and Burton, R., "Application of a Quadruple Probe Technique to MPD Thruster Plume Measurements," *Journal of Propulsion and Power*, Vol. 9, No. 5, 1996, pp. 771–77.

[11]Eckman, R., Byrne, L., Gatsonis, N., and Pencil, E., "Triple Langmuir Probe Measurements in the Plume of a Pulsed Plasma Thruster," *Journal of Propulsion and Power*, Vol. 17, No. 4, 2001, pp. 762–771.

[12]Tilley, D., Kelly, A., and Jahn, R., "The Application of the Triple Probe Method to MPD Thruster Plumes," *21st International Electric Propulsion Conference*, 1990, pp. AIAA–90–2667.

[13]Gallimore, A., Kelly, A., and Jahn, R., "Anode Power Deposition in Magnetoplasmadynamic Thrusters," *Journal of Propulsion and Power*, Vol. 9, 1993, pp. 361–368.

[14]Chen, S.-L. and Sekiguchi, T., "Instantaneous DirectDisplay System of Plasma Parameters by Means of Triple Probe," *J. Appl. Phys.*, Vol. 36, 1965, pp. 2363.

[15]Boxman, R. L., Haber, D., and Martin, P. J., *Handbook of Vacuum Arc Science & Technology: Fundamentals and Applications (Materials Science and Process Technology Series)*, Noyes Publications, 1995.

[16]Coulombe, S. and Meunier, J., "Arc-Cold Cathode Interactions: Parametric Dependence on Local Pressure," *Plasma Sources Sci. Technol.*, Vol. 6, 1997, pp. 508–517.

[17]Lu, J., Krier, H., Burton, R., and Goodfellow, K., "Cathode Sheath Voltage Models for Hydrazine Arcjets," *Journal of Thermophysics and Heat Transfer*, Vol. 12, No. 2, 1998, pp. 230–238.

[18]Maecker, H., "Plasma Streaming in Arcs Caused by Self-Magnetic Compression," *Zeitschrift fur Physik*, , No. 139, 1955, pp. 448–463.

[19]Lee, T. and Greenwood, A., "Theory for the Cathode Mechanism in Metal Vapor Arcs," *J. Appl. Phys.*, Vol. 32, 1961, pp. 916–923.

[20]Schrade, H., Auweter-Kurtz, M., and Kurtz, H., "Analysis of the Cathode Spot of Metal Vapor Arcs," *IEEE Transactions on Plasma Science*, 1983, pp. 103–110.

[21]Bohm, D., *The Characteristics of Electrical Discharges in Magnetic Fields*, New York: MacGraw-Hill, 1949.

[22]Murphy, E. and Good, R., "Thermionic Emission, Field Emission, and the Transition Region," *Physical Review*, Vol. 102, 1956, pp. 1464–1473.

[23]Paulini, J., Klein, T., and Simon, G., "Thermo-field Emission and the Nottingham Effect," *J. Phys. D: Appl. Phys.*, Vol. 26, 1993, pp. 1310–15.

[24]Hunter, L. and Kuttler, J., "Enthalpy Method for Ablation-Type Moving Boundaries Problems," *J. Thermophysics*, Vol. 5, 1990, pp. 240–242.

[25]Rossignol, J., Abbaoui, M., and Clain, S., "Numerical Modelling of Thermal Ablation Phenomena Due to a Cathodic Spot," *J. Phys. D: Appl. Phys.*, Vol. 33, 2000, pp. 2079–2086.